CRYSTAL GROWTH & DESIGN

ARTICLE

pubs.acs.org/crystal

Adsorbate Selectivity of Isoreticular Microporous Metal−Organic Frameworks with Similar Static Pore Dimensions

Xinfang Liu, Minhak Oh, and Myoung Soo Lah*

Interdisciplinary School of Green Energy, Ulsan National Institute of Science & Technology, Ulsan, 689-798, Korea

S Supporting Information

ABSTRACT: Adsorbate selectivity has been investigated using three isoreticular metal−organic frameworks (MOFs) {[ML], **1** (M = Cu^{2+}) and **2** (M = Zn^{2+}) where L = 5-(pyridin-3-ylethynyl)isophthalate; **3** (M = Cu^{2+}) where L = [(pyridin-3-ylmethyl)amino] isophthalate} of similar "static aperture size" but of different framework flexibility, where the MOFs have the same two different types of cagelike pores, cage A and cage B. While cage A of the MOFs with sufficiently large aperture size compared with the dimensions of the adsorbates investigated does not show any adsorbate selectivity, cage B with an approximate size match between the adsorbates and the pore apertures shows size selectivity for the adsorbates. Although the static aperture size of cage B in **3** is smaller than those in **1** and **2**, the order of the "effective aperture sizes" of the cage Bs of the activated MOFs, **1a**−**3a**, is **2a** ≥ **3a** ≥ **1a**, which reflects the differing framework flexibility. The size selectivity of the MOFs for N_2 and Ar follows the more shape-dependent second minimum dimension (MIN-2) of the adsorbate rather than the widely used kinetic diameter (KD). However, the size selectivity of the MOFs for CO, CO_2, and O_2 is neither based on the KD nor on the MIN-2. Not only the aperture size but also the functionality of the aperture-constituting group plays a role in the selective adsorption.

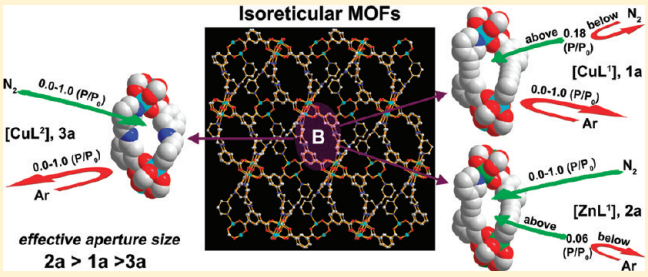

INTRODUCTION

Inorganic porous materials with specific dimensions have been explored as selective adsorbents for various guest molecules.[1] However, it is not easy to tune their selective properties by controlling the size and properties of the pore aperture because of the difficulty in adjusting the constituting inorganic building blocks. The development of porous crystalline materials via metal−organic coordination has attracted tremendous interest because of their tunability, originating from the adjustable structural and functional properties of organic building components.[2]

Recently, we reported two isoreticular microporous MOFs ([ML^1], L^1 = 5-(pyridin-3-ylethynyl)isophthalate, M = Cu^{2+} for **1**; Zn^{2+} for **2**) with two different types of cagelike pores, cage A and cage B,[3] using H_2L^1 as a ligand possessing an isophthalate (iph) unit for a two-dimensional (2-D) Kagomé layer based on a paddle wheel as a secondary building unit (SBU) and the pyridyl unit as an auxiliary connecting residue between the 2-D Kagomé layers, where the two units of the ligand are interconnected via a rigid C−C triply bonded ethynyl group. Small adsorbate gas molecules such as N_2 and Ar could be distinguished by the cage B pores of the MOFs based on the shape-dependent second minimum dimensions (MIN-2s) of the adsorbate gas molecules (MIN-2s: N_2, 3.05 Å; Ar, 3.63 Å)[4,5] rather than the widely used kinetic diameters (KDs) (KDs: N_2, 3.64 Å; Ar, 3.40 Å).[1b,5] Interestingly, although the two isostructural MOFs have cage Bs of the same "static aperture size",[5] their selectivities for the gas molecules are not the same. Cage B of **2** behaves as if it has a larger "effective aperture size"[5] than that of cage B of **1**, which reflects the different extents of the framework flexibility of the MOFs caused by the different metal ions in the SBU.

In this work, we synthesized a new ligand, 5-[(pyridin-3-ylmethyl)amino]isophthalic acid (H_2L^2), by introducing a flexible aminomethylene group as a linking residue between the iph unit and the pyridyl group instead of the rigid C−C triply bonded ethynyl group (Scheme 1) and prepared a new isoreticular MOF, [CuL^2] (**3**), with the same two different types of cagelike pores. The isoreticular MOF constructed using the H_2L^2 ligand could have increased framework flexibility and hence might have a larger effective aperture size of the cage B pore than those of **1** and **2**. The size-selective gas sorption characteristics of three isoreticular MOFs with similar static aperture sizes of the cage B pores but with different framework flexibilities have been investigated using small gas molecules, including N_2 and Ar.

EXPERIMENTAL SECTION

General Procedures. All reagents were purchased from commercial sources and were used without further purification. Elemental analyses were conducted on an elemental analyzer, Flash 2000, at the Ulsan National Institute of Science & Technology, Korea. Mass spectral data were obtained on a Jeol JMS 700 high-resolution mass spectrometer (HRMS) at the Korea Basic Science Institute (Daegu). FT−IR spectra were recorded as KBr pellets with a Varian 1000 FT−IR spectrophotometer

Received: July 29, 2011
Revised: September 5, 2011
Published: September 06, 2011

Scheme 1. The Two Ligands, 5-(Pyridin-3-ylethynyl) isophthalic Acid (H_2L^1) and 5-[(Pyridin-3-ylmethyl)amino] isophthalic Acid (H_2L^2), with the Different Linking Moieties, Ethynyl and Aminomethylene Groups

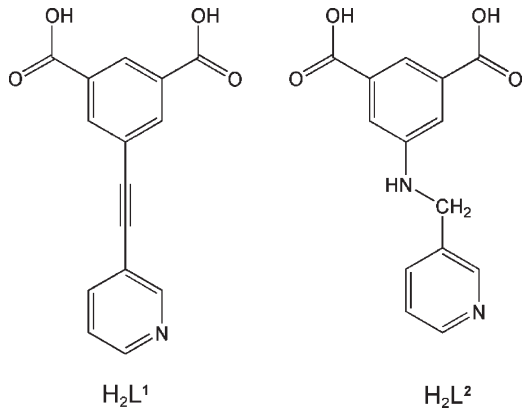

(4000−400 cm^{-1}). Nuclear magnetic resonance (NMR) spectra were obtained on a Varian-600 NMR spectrometer. Powder X-ray diffraction (PXRD) data were recorded using a Rigaku D/M 2200T automated diffractometer at room temperature with a step size of 0.02° in 2θ angle. The variable temperature PXRD (VT-PXRD) measurements were carried out in air using a Rigaku D/M 2500T automated diffractometer. Samples were gradually heated from room temperature with a holding time of at least 30 min at each temperature. Simulated PXRD pattern was calculated with the Material Studio program[6] using the single-crystal structure.

Preparation of 5-[(Pyridin-3-ylmethyl)amino]isophthalic Acid (H_2L^2). Triethylamine (2.8 mL, 20 mmol) was added to a mixture of 5-aminoisophthalic acid (0.910 g, 5.02 mmol) and 3-pyridinecarboxaldehyde (0.47 mL, 5.0 mmol) in 50 mL of anhydrous methanol. After stirring for 5 h, an excess amount of $NaBH_4$ (0.95 g, 25.11 mmol) was slowly added to the solution. The solution was further stirred for an additional 12 h at 4 °C, and then the solution was concentrated using a rotary evaporator. The residue was dissolved in water (50 mL) and acidified with acetic acid to pH 5−6. A pale pinkish solid product was filtered and air-dried. Yield = 1.28 g, 93.8%. HRMS (FAB) m/z calcd for $C_{14}H_{13}N_2O_4$ $[M + 1]^+$ 273.0875, found 273.0873; IR spectrum (KBr, cm^{-1}): 3374(w), 2983(w), 2944(w), 2883(w), 1643(s), 1589(s), 1504(m), 1440(m), 1367(s), 1309(m), 1267(m), 1214(w), 1105(w), 1018(w), 887(w), 823(m), 788(w), 748(s), 703(w), 659(w); ^{1}H NMR spectrum (600 MHz, DMSO-d_6, δ ppm): 12.90 (s, 2H, −COOH), 8.59 (s, 1H, Py−H), 8.45 (d, 1H, Py−H), 7.75 (d, 1H, Py−H), 7.69 (t, 1H, Py−H), 7.37 (d, 2H, Ar−H), 7.35 (t, 1H, Ar−H), 6.84 (t, 1H, −NH−), 4.39 (d, 2H, $-CH_2-$); ^{13}C NMR spectrum (150 MHz, DMSO-d_6, δ ppm): 167.13, 148.80, 148.72, 148.18, 135.05, 134.89, 131.83, 123.63, 117.88, 116.68, 43.96.

Preparation of [CuL^1]·xDMA·yH$_2$O, ***1*** *and [ZnL^1]·xDEF·yH$_2$O,* ***2***. (x and y are the numbers of solvent molecules; DMA = *N,N*-dimethylacetamide; DEF = *N,N*-diethylformamide): **1**, **2**, and the corresponding activated samples, **1a** and **2a**, were prepared according to the literature procedures.[3]

Preparation of [CuL^2]·xDMA·yH$_2$O, ***3***. (x and y are the numbers of solvent molecules): A solution of $Cu(NO_3)_2 \cdot 2.5H_2O$ (0.0092 g, 0.04 mmol) was mixed with H_2L^2 (0.0054 g, 0.02 mmol) in 0.80 mL DMA. To this was added 0.015 mL of HCl (concentrated HCl/H_2O (v/v): 1/5), with stirring. The mixture was sealed in a Pyrex tube and heated to 100 °C for 1 day. The green hexagonal plate crystals obtained were filtered and washed with DMA, and then air-dried to yield 0.0049 g of product, **3**. IR spectrum (KBr, cm^{-1}): 3330(m), 2934(m), 1630(s), 1606(s), 1575(m), 1433(s), 1376(s), 1287(m), 1263(m), 1190(m), 1146(w), 1109(w), 1054(w), 1033(w), 1014(m), 912(w), 875(w), 803(w), 776(s), 730(s), 709(m), 668(w), 647(w), 591(w), 485(m). Because the extent to which the solvent molecules occupy the cavity of **3** varies depending on the exposure time of the sample to air, **3a** was prepared by repeatedly soaking and desolvating **3** in methylene chloride (MC), and then by vacuum-drying at room temperature for 24 h to yield 0.0041 g of product (62% yield based on the ligand). Elemental analysis was carried out on the sample of air-exposed **3a**. Calcd for $[CuL^2] \cdot 2H_2O$, ($C_{14}H_{14}N_2O_6Cu$, fw = 369.82): C 45.47, H 3.82, N 7.57%; found: C 45.81, H 3.42, N 7.66%.

Table 1. Crystal Data and Structure Refinement for 3

empirical formula	$C_{14}H_{10}N_2O_4Cu$
formula weight	333.78
temperature (K)	99(2)
wavelength (Å)	0.80000
space group	$R\bar{3}c$
unit cell dimensions (Å)	$a = b = 18.621(3)$
	$c = 69.793(14)$
volume (Å^3)	20957(6)
Z	36
D_{calcd} (g·cm^{-3})	0.952
μ (mm^{-1})	0.948
$F(000)$	6084
total/unique reflections	42746, 4766
R_{int}	0.0565
R_1, wR_2 [$I > 2\sigma(I)$]	0.0734, 0.2157
R_1, wR_2 (all data)	0.0785, 0.2209
goodness-of-fit	1.072
difference Fourier map, max, min (e·Å^{-3})	1.778, −0.787

Crystallographic Data Collection and Refinement of Structures. A single crystal of **3** was coated with paratone oil and the diffraction data measured at 99 K with synchrotron radiation (λ = 0.80000 Å) on a 6BMXW ADSC Quantum-210 detector with a Pt-coated Si double crystal monochromator at the Pohang Accelerator Laboratory, Korea. The ADSC Quantum-210 ADX program[7] was used for data collection and HKL2000 (Ver. 0.98.698a)[8] was used for cell refinement, reduction, and absorption correction. The structure was solved by direct methods and refined by full-matrix least-squares calculations with the SHELXTL software package.[9]

One copper cation and one ligand were observed as an asymmetric unit. The pyridyl residue of the ligand was statistically disordered. All nonhydrogen atoms were refined anisotropically; only the hydrogen atoms attached to the ligand were assigned isotropic displacement coefficients U(H) = 1.2U (C, N) and their coordinates were allowed to ride on their respective atoms. The refinement converged to R_1 = 0.1027 and wR_2 = 0.3215 for 4097 reflections with $I > 2\sigma(I)$. Structure refinement after modification of the data for the disordered solvent region (10322 Å^3, 49.3% of the crystal volume) with the SQUEEZE routine of PLATON[10] led to better refinement and data convergence. Refinement of the structure converged to a final R_1 = 0.0734 and wR_2 = 0.2157 for 4134 reflections with $I > 2\sigma(I)$; R_1 = 0.0785 and wR_2 = 0.2209 for all reflections. The largest difference peak and hole were 1.778 and −0.787 e·Å^{-3}, respectively.

A summary of the crystallographic data is given in Table 1. CCDC-795323 contains the supplementary crystallographic data for **3**. The data can be obtained free of charge at www.ccdc.cam.ac.uk/conts/retrieving.html or from the Cambridge Crystallographic Data Centre, 12, Union Road, Cambridge CB2 1EZ, UK.

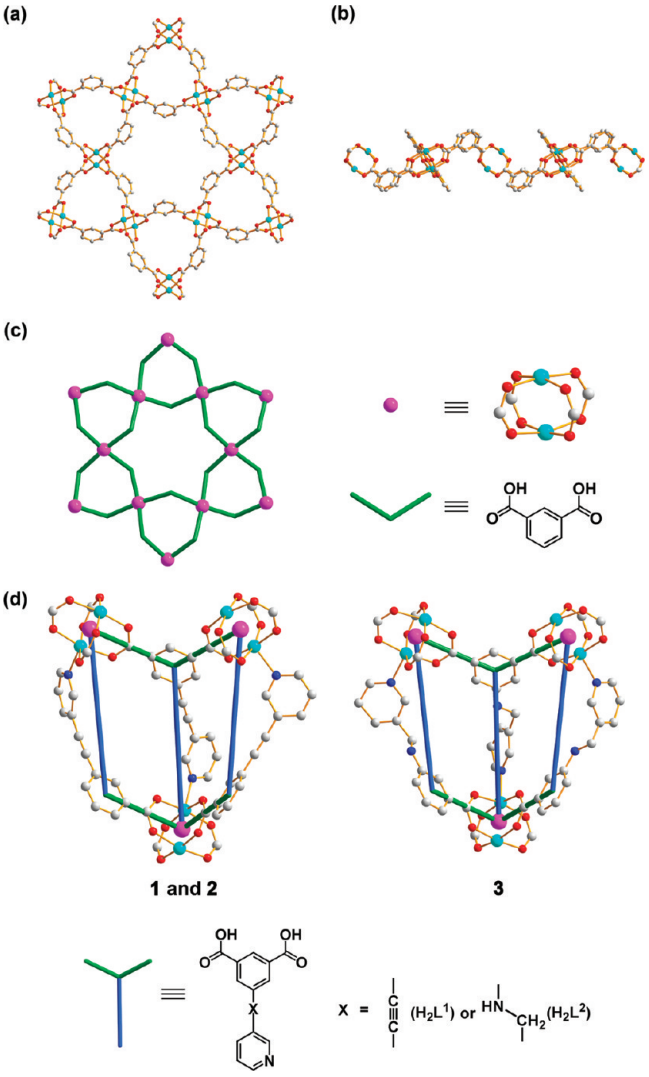

Figure 1. (a, b) Ball-and-stick diagrams showing a 2-D Kagomé layer along the crystallographic *c*-axis and the crystallographic *b*-axis, respectively. (c) A schematic diagram of a 2-D Kagomé layer. (d) Ball-and-stick diagrams showing the coordination of pyridyl groups to the fifth coordination site of the metal centers of the paddle-wheel SBUs of the neighboring 2-D Kagomé layers in **1**/**2** and **3**, respectively.

Low-Pressure Gas Sorption Measurements. All gas sorption isotherms were measured using a BELSORP-max (BEL Japan, Inc.) with a standard volumetric technique up to saturated pressure. The N_2 (with purity of 99.999%) and the CO (99.998%) sorption isotherms were monitored at 77 K. The Ar (with purity of 99.9999%) and the O_2 (99.99%) sorption isotherms were measured at 87 K. The CO_2 (99.99%) sorption isotherms were measured at 195 K. The adsorption data in the pressure range lower than ~0.1 P/P_0 were fitted to the Brunauer–Emmett–Teller (BET) equation to determine the BET surface areas. For the Langmuir surface areas, data from the whole adsorption data were used. The H_2 (99.999%) sorption isotherms were measured at both 77 and 87 K.

RESULTS AND DISCUSSION

A solvothermal reaction of H_2L^2 with $Cu(NO_3)_2 \cdot 2.5H_2O$ in DMA in the presence of a small amount of HCl gave a Cu MOF, **3**, that is isoreticular to the reported MOFs, **1** and **2**. However, similar reactions of H_2L^2 with Zn(II) ion only led to two different 2-D layered Zn MOFs with the same honeycomb net topology rather than an isoreticular Zn MOF structure.[11]

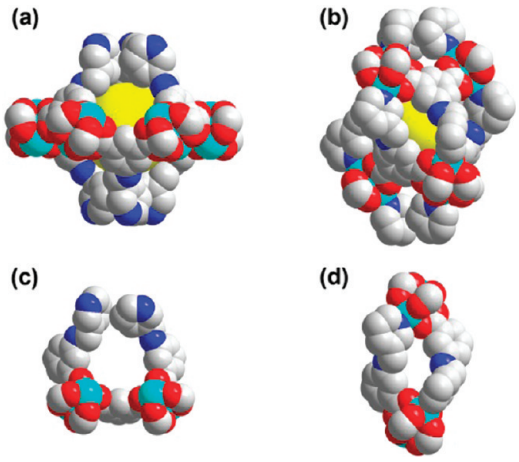

Figure 2. Space-filling models of the two cagelike pores of **3**. (a) The cage A pore with the diameter of ~10 Å. (b) The cage B pore with the diameter of ~8.0 Å. (c) The aperture of the cage A pore. (d) The aperture of the cage B pore. The large yellow balls in the centers of the cages are dummy balls representing the approximate pore dimensions of the cagelike pores.

The single-crystal X-ray diffraction analysis revealed that **3**, as in the case of **1** and **2**, was a three-dimensional (3-D) MOF (Figures S1 and 1; Table 1) with two different types of cagelike pores (Figure 2), where the 3-D network was generated by the pillaring of the internal pyridyl residue between the 2-D layers of the Kagomé net topology. The pore diameters of cages A and B in **3** are ~10 Å and ~8.0 Å, respectively. The diameter of the circular aperture in the D_3-symmetric cage A is ~6 Å. However, the static aperture size of the D_3-symmetric cage B, even in its largest possible dimensions in the disordered model (Figure S2),[12] is slightly smaller than those in **1** and **2**, i.e., ~2.3 Å in its shortest dimension and ~5.4 Å in its longest dimension (Figures 3 and S3; Table 2). The flexible aminomethylene moiety of H_2L^2 with larger steric volume compared with the rigid straight ethynyl moiety of H_2L^1 with the smaller steric volume results in smaller static aperture size of cage B in **3** than those in **1** and **2**.

The PXRD pattern of as-synthesized **3** indicates that the single crystal is representative of the bulk sample (Figure 4). **3** is thermally stable at least up to 250 °C (Figure 5). Even the activated sample, **3a**, prepared by repeatedly soaking and desolvating **3** in MC and then vacuum drying at room temperature for 24 h, is stable in air. Thermogravimetric analysis (TGA) of the activated sample indicates the presence of some solvent in the pore (Figure S4, Supporting Information); however, we believe that this solvent is water molecule adsorbed into the pore from air when the activated sample was exposed in air for the TGA experiment. The amounts of the reabsorbed water molecules vary up to two water molecules per formula unit depending on the exposure time of the activated sample in air. The PXRD pattern of the air-exposed activated sample did not indicate loss of its crystallinity (Figure 4).

In contrast to the clear two-step N_2 adsorption isotherm of **1a** and the distinctive stepwise Ar adsorption isotherm of **2a**,[3] **3a** shows typical type I adsorption isotherms for both N_2 at 77 K and

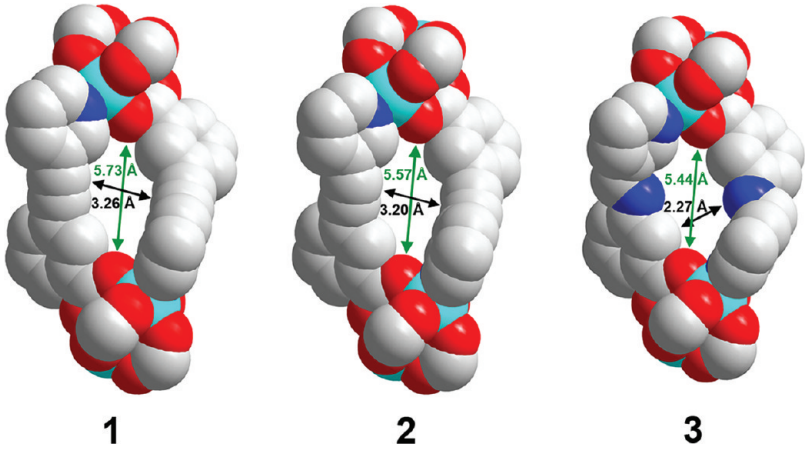

Figure 3. The static aperture dimensions of the cage B pores in **1**, **2**, and **3**.

Table 2. The Static Aperture Dimensions (Å) of the Two Cagelike Pores, Cage A and Cage B, in the MOFs[a]

	1[3]	2[3]	3[b]
cage A	H(C4)···H(C11) 6.16	H(C4)···H(C11) 6.35	H(C5)···H (C7)[c] 6.06
	H(C9)···H(C13) 5.45	H(C9)···H(C9) 5.83	H(C12)···H(C3)[d] 5.97
cage B	O4···O2 5.73	O2···O2 5.57	O2···O4[e] 5.44
	C6···C6 3.26	C6···C6 3.20	H(C7)···H(N1)[e] 2.27

[a] The static aperture dimensions have been calculated from the interatomic distances considering the van der Waals radii of the constituting atoms. The van der Waals radii used for C, H, N, and O are 1.77, 1.10, 1.64, and 1.58 Å, respectively.[13] [b] The cage dimensions for **3** have been calculated from the structure with the disordered model having the largest possible aperture dimensions. Symmetry codes: (c) $1-y, x-y, z$. (d) $1/3+y, -1/3+x, 1/6-z$. (e) $2/3+x-y, -2/3+x, 1/3-z$.

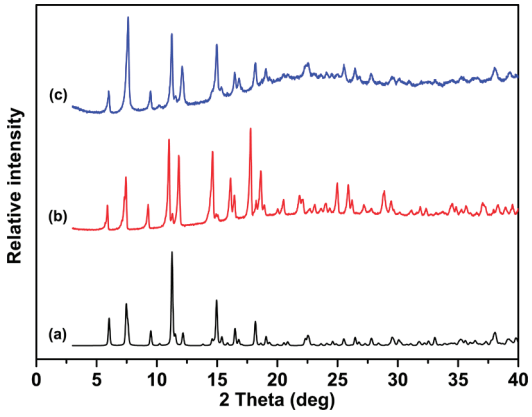

Figure 4. PXRD patterns of **3**. (a) A simulated PXRD pattern from the single-crystal structure of **3**. (b) As-synthesized bulk sample of **3**. (c) **3a**, the sample prepared via soaking **3** in MC and then vacuum-drying at room temperature for 24 h.

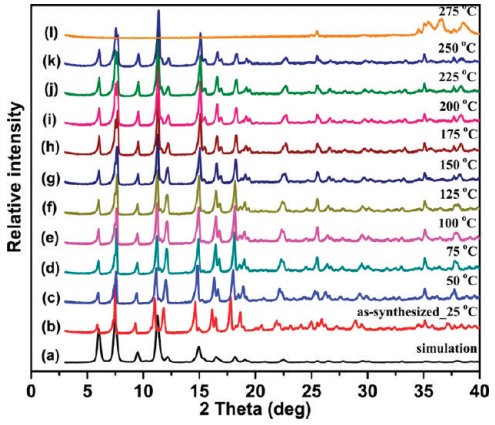

Figure 5. VT-PXRD patterns of **3**. (a) The simulated pattern from a single-crystal structure of **3**; (b) as-synthesized, **3** at 25 °C; then heated to (c) 50 °C; (d) 75 °C; (e) 100 °C; (f) 125 °C; (g) 150 °C; (h) 175 °C; (i) 200 °C; (j) 225 °C; (k) 250 °C; (l) 275 °C.

Ar at 87 K at 1 atm (Figure 6). The amounts of N_2 and Ar adsorbed in the pores of the framework are ~392 $cm^3\ g^{-1}$ and ~427 $cm^3\ g^{-1}$, respectively, and the BET surface area and Langmuir surface area of 1430 and 1620 $m^2\ g^{-1}$ calculated using the Ar adsorption isotherm are slightly smaller than the corresponding values obtained based on the N_2 adsorption isotherm, 1490 and 1690 $m^2\ g^{-1}$, respectively. Noticeably, the specific pore volume occupied by Ar, 0.542 $cm^3\ g^{-1}$, is smaller than the specific pore volume occupied by N_2, 0.605 $cm^3\ g^{-1}$ (Table 3).[14]

The difference in the specific pore volumes occupied by the two adsorbates, Ar and N_2, suggests that Ar is only allowed into the pores of cage A but not allowed into the pores of cage B, while N_2 is allowed into the pores of both cage A and cage B. The selectivity of cage B in **3a** for the adsorbates, N_2 and Ar, is not based on their KDs (N_2, 3.64 Å; Ar, 3.40 Å) but based on their MIN-2s (N_2, 3.05 Å; Ar, 3.63 Å) as with the selectivities of the cage Bs in **1a** and **2a**. In addition to the selectivity of the cage Bs

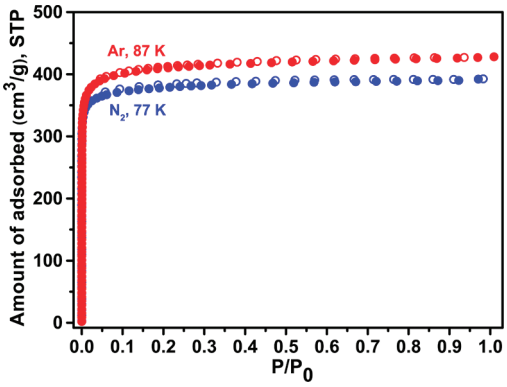

Figure 6. N_2 and Ar sorption isotherms on **3a**. Color codes: N_2 sorption isotherm at 77 K (blue); Ar sorption isotherm at 87 K (red). Filled circles represent the adsorption amounts and open circles represent the desorption amounts.

Table 3. The Specific Pore Volumes ($cm^3\ g^{-1}$) Calculated Based on the Gases Adsorbed for 1a, 2a, and 3a

	1a	2a	3a
Ar, 87 K	0.594[3]	0.660[3]	0.542
O_2, 87 K	0.641	0.652	0.588
N_2, 77 K	0.696[3]	0.667[3]	0.605
CO, 77 K	0.693	0.666	0.619
CO_2, 195 K	0.636	0.646	0.583

based on the MIN-2 values of the adsorbates, these observations indicate that the effective aperture size of cage B in **3a** is smaller than the dimension of Ar but larger than that of N_2. Even the largest possible static aperture size of the pores of cage B calculated from the disordered model of the crystal structure **3a** is smaller than the static aperture sizes of the pores of cage Bs calculated based on the crystal structures of **1a** and **2a**. However, the effective aperture size of **3a** is larger than that of **1a** but smaller than that of **2a**. The effective aperture size of cage B could be estimated from the dimension of the adsorbate showing stepwise sorption behavior. The stepwise N_2 sorption behavior in **1a** and the similar stepwise Ar sorption behavior in **2a** show that the effective aperture size of cage B in **1a** is comparable with the MIN-2 value of N_2 and the effective aperture size of cage B in **2a** is comparable with the MIN-2 value of Ar. When these observations are combined with the fact that the effective aperture size of cage B in **3a** is smaller than the dimension of Ar but larger than that of N_2, the order of the effective aperture sizes of cage Bs is **2a** (~ MIN-2 value of Ar) ≥ **3a** ≥ **1a** (~ MIN-2 value of N_2), which does not agree with the expected order from the static aperture size of the frameworks based on the single-crystal structures (**1a** ≥ **2a** > **3a**). The discrepancy could be explained using the different extents of the framework flexibilities, mainly attributed to the different ligand flexibilities and the different flexibilities of the metal coordination environments.

To investigate the size selectivity of the three isoreticular MOFs for other small adsorbates, the sorption behaviors of O_2 (KD = 3.46 Å; MIN-2: 2.985 Å), CO (KD = 3.76 Å; MIN-2: 3.339 Å), and CO_2 (KD = 3.30 Å; MIN-2: 3.339 Å) have been investigated (Figures 7 and S5−S13).

For **1a**, although the stepwise behaviors in the O_2 and CO adsorption isotherms are not as clear as that of the N_2 adsorption isotherm, the logarithmic plots of the isotherms indicate gentle steps in the pressure range of 0.05−0.1 P/P_0 (Figures 7, S5 and S6). The dimensions of the O_2 and CO molecules are also comparable to the effective aperture size of cage B, as in the case of the N_2 molecule. The accessible specific pore volumes from the adsorption isotherms of CO, O_2, and CO_2 molecules were similarly estimated as in the cases of N_2 and Ar, assuming the density of the adsorbate in the pore to be the same as that of the corresponding liquid-state adsorbate at the given temperature ($d_{O2,87\ K}$ = 1.157 g cm^{-3}; $d_{CO,77\ K}$ = 0.813 g cm^{-3}; $d_{CO2,195\ K}$ = 1.18 g cm^{-3}) (Figures 7 and S7; Table 3). The total accessible specific pore volume (0.693 $cm^3\ g^{-1}$) and the accessible specific pore volume (~ 0.1 $cm^3\ g^{-1}$) above the threshold pressure (~ 0.05 P/P_0) estimated from the CO adsorption isotherm also suggest that CO molecules could access the cage B pore. Even though the total accessible pore volume (0.641 $cm^3\ g^{-1}$) estimated from the O_2 adsorption isotherm is slightly smaller than those estimated from the N_2 and CO adsorption isotherms, the similar ratio of the total accessible pore volume and the accessible pore volume (~0.1 $cm^3\ g^{-1}$) above the threshold pressure ~ (0.1 P/P_0) indicates that the cage B pore could also be accessed by O_2 molecules. There is an ambiguity in the accessibility of CO_2 molecules to the pore of the cage B from the sorption isotherms. The CO_2 sorption isotherms do not show any stepwise sorption behavior, and the specific pore volume (0.636 $cm^3\ g^{-1}$) estimated from the CO_2 sorption isotherms is smaller than those estimated from the N_2 and CO sorption isotherms but larger than that estimated from the Ar sorption isotherm. Hence, the dimension of the CO_2 molecule could not be assessed based on the accessibility to the pores of the cage B. The dimensions of the adsorbates based on the sorption behaviors on **1a** are in the order of Ar > O_2 ≈ N_2 ≈ CO.[15] The effective aperture size of cage B is smaller than the dimension of Ar but comparable to those of N_2, O_2, and CO molecules.

For **2a**, the O_2 sorption isotherm also shows a gentle step at a pressure of ~0.2 P/P_0 with some hysteresis that again reflects some degree of framework flexibility (Figures 7, S8, and S9). The combination of stepwise behavior and total specific pore volume (0.652 $cm^3\ g^{-1}$) indicates that the O_2 molecule can access the pores of cage B and the dimension of O_2 also approximately matches the effective aperture size of cage B (Figure S10). The lack of a clear stepwise behavior in the sorption isotherms of CO and CO_2 molecules and their total specific pore volumes (0.666 $cm^3\ g^{-1}$ and 0.646 $cm^3\ g^{-1}$, respectively) show that both molecules can access the cage B pores over the whole pressure range and their dimensions are smaller than the effective aperture size of cage B. The dimensions of the adsorbates based on the sorption behaviors in **2a** are in the order of Ar ≈ O_2 > N_2, CO, CO_2. Although the dimension of the CO_2 molecule could not be assessed from the sorption study on **1a** because of the uncertainty in the accessibility of adsorbate CO_2 to the pores of cage B, the fact that the dimension of CO_2 is smaller than that of O_2 from the sorption study on **2a** shows that the combined order of the dimensions of the adsorbates is Ar ≥ O_2 ≥ N_2 ≈ CO, CO_2.

Sorption measurements for O_2, CO, and CO_2 gases on **3a** were also carried out to understand its size-selective sorption behavior (Figures 7 and S11−S13). The O_2 sorption isotherm in its logarithmic plot also shows a gentle step in the pressure range

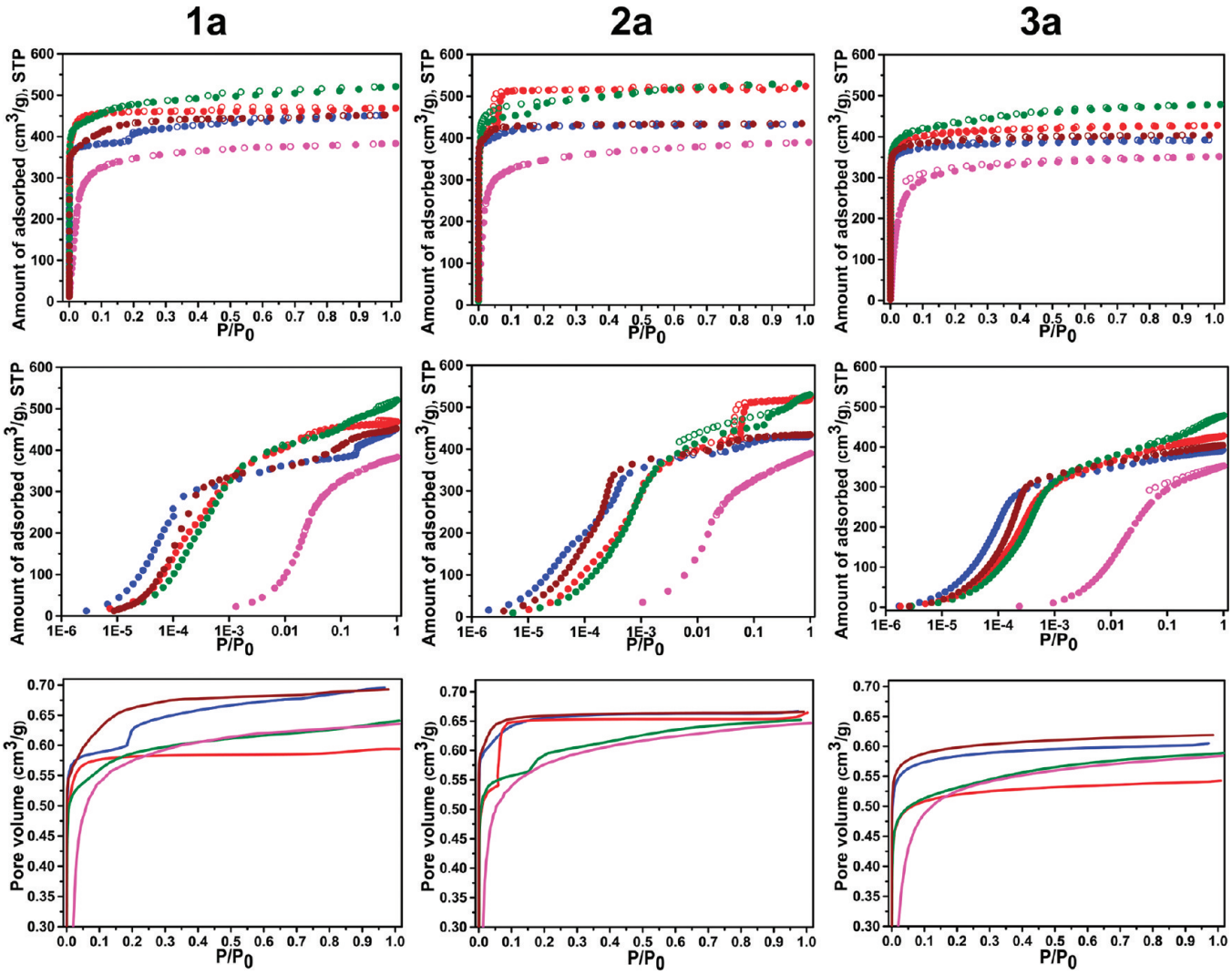

Figure 7. Top: N_2, Ar, O_2, CO, CO_2 sorption isotherms of **1a**, **2a**, and **3a**. Middle: sorption isotherms plotted against logarithmic relative pressure. Bottom: specific pore volumes of the frameworks occupied by the adsorbates. Filled circles represent the adsorption amounts and open circles represent the desorption amounts. Color codes: N_2 at 77 K (blue); Ar at 87 K (red); O_2 at 87 K (green); CO at 77 K (brown); CO_2 at 195 K (magenta).

of 0.05−0.3 P/P_0 with no hysteresis, even though the framework has some degree of flexibility. The percentage of the pore volume calculated after the step compared with the total pore volume is ∼0.15%, which suggests that O_2 can access the pores of cage B after the threshold pressure and the effective aperture size of cage B in **3a** is similar to the dimension of the O_2 molecule. No stepwise behavior and the total specific pore volumes in the sorption isotherms of CO and CO_2 on **3a** as in the case of the isotherms of the same adsorbates on **2a** suggest that the adsorbates can go into the pores of cage B and the dimensions of the adsorbates are smaller than the effective aperture size of cage B.

The dimensions of the adsorbates based on the sorption behavior in **3a** are in the order of Ar > O_2 > N_2, CO, CO_2. This order also agrees with the combined order from the sorption studies on **1a** and **2a**, Ar ≥ O_2 ≥ N_2 ≈ CO, CO_2, where the order of the dimensions between N_2 ≈ CO and CO_2 could not be determined based on the current work.[15] The order of the relative dimensions of Ar and N_2 is quite reliable based on the sorption behaviors and the total specific pore volumes for both Ar and N_2 on these three isoreticular MOFs. However, the combined order of the adsorbates' dimensions follows neither the order based on the widely used KD values (CO > N_2 > O_2 > Ar > CO_2) nor the order based on the more shape-dependent MIN-2 values (Ar > CO ≈ CO_2 > N_2 > O_2).

The hydrogen storage capability of **3a** is close to those of **1a** and **2a** (Figure 8). The hydrogen uptake amount on **3a** was 2.36 wt % at 77 K and 1 bar. The isosteric heat of adsorption calculated from the H_2 isotherms at 77 and 87 K using the virial method[16] is in the range 7.24−6.25 kJ mol^{-1} for **3a** (coverage of 0.02−1.68 wt % H_2 uptake) depending on the degree of H_2 loading (Figure 8b). The relatively high isosteric heats of hydrogen adsorption on **3a** might come from the small pore diameters and the narrow and meandering channel structure of the MOF as the cases of **1a** and **2a**. The difference in the isosteric heats of adsorption, ∼ 0.5 kJ/mol, between the isosteric heat of adsorption on **3a** and the isosteric heats of adsorption on **1a** and **2a** might reflect the difference in their average pore diameters. Although all of the structures are isoreticular and have the similar unit cell volumes, the reduced pore percentages in **3a** compared

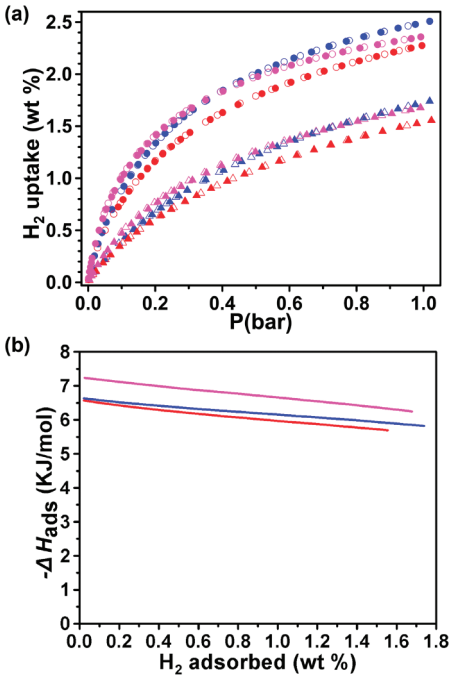

Figure 8. (a) H_2 sorption isotherms on **1a**, **2a**, and **3a** at 77 K (circles) and 87 K (triangles), respectively; (b) H_2 adsorption enthalpies on **1a**, **2a**, and **3a**. Color codes: **1a** (blue), **2a** (red), **3a** (magenta). Filled shapes represent the adsorption amounts and open shapes represent the desorption amounts.

with **1a** and **2a** that originated from the increased steric volume of H_2L^2 relative to H_2L^1 might be responsible for the reduced average pore diameter and the consequent increased isosteric heat of H_2 adsorption on **3a** compared with those on **1a** and **2a**.

CONCLUSIONS

A new isoreticular 3-D MOF, **3**, with two different cagelike pores was prepared using H_2L^2 containing an aminomethylene group as an internal auxiliary pillaring linker of increased flexibility. While cage A pores of the MOF with sufficiently large aperture size compared with the size of the adsorbates, N_2 and Ar, do not show any size selectivity, cage B pores with an approximate size match between the adsorbates and the pore aperture show size selectivity based not on the KDs of the adsorbates (N_2, 3.64 Å; Ar, 3.40 Å) but on the more shape-dependent MIN-2s of the adsorbates (N_2, 3.05 Å; Ar, 3.63 Å). The selectivity of cage B for the adsorbates does not follow the static aperture size but follows the effective aperture size, which reflects the extent of the framework flexibility. Although the static aperture size of cage B in **3** is smaller than those in **1a** and **2a**, the order of the effective aperture sizes is **2a** (~ MIN-2 of Ar) ≥ **3a** ≥ **1a** (~ MIN-2 of N_2).

However, three isoreticular microporous MOFs with slightly different effective aperture sizes of cage Bs distinguish the small adsorbates (Ar/O_2/N_2/CO/CO_2) based neither on the widely used KDs of the adsorbates (the order based on the KD values: CO (3.76 Å) > N_2 (3.64 Å) > O_2 (3.46 Å) > Ar (3.40 Å) > CO_2 (3.30 Å)) nor on the MIN-2s (the order based on the MIN-2 values: Ar (3.76 Å) > CO (3.339 Å) ≈ CO_2 (3.339 Å) > N_2 (3.054 Å) > O_2 (2.985 Å)). The observed order of the dimensions of the small adsorbates based on the sorption study is Ar ≥ O_2 ≥ N_2 ≈ CO, CO_2. This suggests that not only the aperture size of the pores but also the functionality of the aperture-constituting groups might play an important role in the selective adsorption of even small and simple adsorbate molecules.

ASSOCIATED CONTENT

Supporting Information. Packing diagrams of **3** in ball-and-stick and space-filling models; three possible aperture dimensions of cage B pore of **3** in the disordered model; ball-and-stick drawings of the two cagelike pores of **3**; the sorption isotherms in linear and logarithmic scales, and the corresponding specific pore volumes of **1a**, **2a**, and **3a**; X-ray crystallographic file (CIF) for **3**. This material is available free of charge via the Internet at http://pubs.acs.org/.

AUTHOR INFORMATION

Corresponding Author

*Phone: 82-52-217-2931; fax: 82-52-217-2019; e-mail: mslah@unist.ac.kr.

ACKNOWLEDGMENT

This work was supported by NRF-2010-0019408 and WCU programs (R31-2008-000-20012-0) through the National Research Foundation of Korea. The authors acknowledge PAL for beam line use (2010-2063-08).

REFERENCES

(1) (a) Yang, R. T. *Adsorbent: Fundamentals and Applications*; John Wiley & Sons: Hoboken, 2003. (b) Beck, D. W. *Zeolite Molecular Sieves*; John Wiley & Sons: New York, 1974. (c) Schuth, F.; Sing, K. S. W.; Weitkamp, J. *Handbook of Porous Solids*; Wiley-VCH: New York, 2002. (d) Wright, P. A. *Microporous Framework Solids*; RSC Publishing: Cambridge, 2008. (e) Tedds, S.; Walton, A.; Broom, D. P.; Book, D. *Faraday Discuss.* **2011**, *151*, 75–94. (f) Ma, S.; Zhou, H.-C. *Chem. Commun.* **2010**, *46*, 44. (g) Morris, R. E.; Wheatley, P. S. *Angew. Chem., Int. Ed.* **2008**, *47*, 4966.(h) Whyte, T. E.; Yon, C. M.; Wagener, E. H. *Industrial Gas Separation*; American Chemistry Society; Washington, DC, 1983.

(2) (a) Li, J.-R.; Kuppler, R. J.; Zhou, H.-C. *Chem. Soc. Rev.* **2009**, *38*, 1477. (b) Zou, R.; Abdel-Fattah, A. I.; Xu, H.; Zhao, Y.; Hickmott, D. D. *CrystEngComm* **2010**, *12*, 1337. (c) Kuppler, R. J.; Timmons, D. J.; Fang, Q.-R.; Li, J.-R.; Makal, T. A.; Young, M. D.; Yuan, D.; Zhao, D.; Zhuang, W.; Zhou, H.-C. *Coord. Chem. Rev.* **2009**, *253*, 3042. (d) Murray, L. J.; Dincă, M.; Long, J. R. *Chem. Soc. Rev.* **2009**, *38*, 1294. (e) Mueller, U.; Schubert, M.; Teich, F.; Puetter, H.; Schierle-Arndt, K.; Pastré, J. *J. Mater. Chem.* **2006**, *16*, 626.(f) Eubank, J. F.; Wojtas, L.; Hight, M. R.; Bousquet, T.; Kravtsov, V. C.; Eddaoudi, M. *J. Am. Chem. Soc.* DOI: 10.1021/ja203898s. (g) Zhang, Z; Wojtas, L.; Zaworotko, M. J. *Cryst. Growth Des.* **2011**, *11*, 1441. (h) Bourne, S. A.; Lu, J.; Mondal, A.; Moulton, B.; Zaworotko, M. J. *Angew. Chem., Int. Ed.* **2001**, *40*, 2111. (i) Chen, B.; Xiang, S.; Qian, G. *Acc. Chem. Res.* **2010**, *43*, 1115. (j) Zhang, Z.; Xiang, S.; Chen, B. *CrystEngComm* DOI: 10.1039/c1ce05437f.

(3) Liu, X.; Oh, M.; Lah, M. S. *Inorg. Chem.* **2011**, *50*, 5044.

(4) (a) Webster, C. E.; Drago, R. S.; Zerner, M. C. *J. Am. Chem. Soc.* **1998**, *120*, 5509. (b) Webster, C. E.; Cottone, A.; Drago, R. S. *J. Am. Chem. Soc.* **1999**, *121*, 12127.

(5) The "kinetic diameter" of an adsorbate is the intermolecular distance of closest approach for two molecules colliding with zero initial kinetic energy,[1b] and the "second minimum dimension (MIN-2)" of an adsorbate is the second smallest dimension of the three-dimensional adsorbate in low energy conformations or molecular orientations that enable the adsorbate to enter a cylindrical pore.[4a] The "static aperture

size" is the aperture dimension observed in solid state crystal structure and could be calculated from the interatomic distances of pore aperture constituting atoms considering the van der Waals radii of the atoms. The "effective aperture size" is the maximum aperture size reflecting the aperture flexibility at a given condition and could be estimated from the dimension of an adsorbate showing stepwise sorption behavior in adsorption experiment.

(6) *Materials Studio Program*, version 4.3; Accelrys: San Diego, CA, 2008.

(7) Arvai, A. J.; Nielsen, C. *ADSC Quantum-210 ADX Program*; Area Detector System Corporation: Poway, CA, USA, 1983.

(8) Otwinowski, Z.; Minor, W. In *Methods Enzymology*; Carter, C. W., Jr., Sweet, R. M., Eds.; Academic Press: New York, 1997; Vol. 276, part A, pp 307−326.

(9) Sheldrick, G. M. *SHELXTL-PLUS, Crystal Structure Analysis Package*; Brucker Analytical X-ray: Madison, WI, 1997.

(10) PLATON program: Spek, A. L. *Acta Crystallogr., Sect. A* **1990**, *46*, 194.

(11) Two MOFs were prepared via solvothermal reactions of equivalent amounts of $Zn(NO_3)_2 \cdot 6H_2O$ and H_2L^2 in 1.00 mL of *N, N*-diethylacetamide at 85 °C for 2 days and at 105 °C for 2 days, respectively. The manuscript is in preparation for publication elsewhere.

(12) The statistically disordered pyridyl group of the ligand leads to three different cage B apertures and hence three different aperture dimensions.

(13) Rowland, R. S.; Taylor, R. *J. Phys. Chem.* **1996**, *100*, 7384.

(14) The specific pore volume of the adsorbent was estimated from the adsorption isotherm assuming that the density of the adsorbate in the pore at a given temperature and at its saturation pressure is the same as that of the adsorbate in its liquid state at the given temperature.

(15) We could not rule out the possibility of the wrong ordering of the relative dimensions of the adsorbates, O_2, CO, and CO_2, because of the less clear or absent stepwise behavior in their sorption isotherms and of the uncertainties in their specific pore volumes, which come from the possibility of framework contraction and expansion during the adsorption processes and/or come from the inaccuracy of the assumed densities of the adsorbates in the pores based on the densities of the adsorbates in their liquid state.

(16) (a) Cole, J. H.; Everett, D. H.; Marshall, C. T.; Paniego, A. R.; Powl, J. C.; Rodriguez-Reinoso, F. *J. Chem. Soc., Faraday Trans.* **1974**, *70*, 2154. (b) O'Koye, I. P.; Benham, M.; Thomas, K. M. *Langmuir* **1997**, *13*, 4054. (c) Reid, C. R.; O'Koye, I. P.; Thomas, K. M. *Langmuir* **1998**, *14*, 2415. (d) Reid, C. R.; Thomas, K. M. *Langmuir* **1999**, *15*, 3206.